

Unveiling galaxy chemical enrichment mechanisms out to $z \sim 8$ from direct determination of O & Ar abundances from JWST/NIRSPEC spectroscopy

SOURADEEP BHATTACHARYA,^{1,2} MAGDA ARNABOLDI,³ ORTWIN GERHARD,⁴ CHIAKI KOBAYASHI,² AND KANAK SAHA¹

¹*Inter-University Centre for Astronomy and Astrophysics, Ganeshkhind, Post Bag 4, Pune 411007, India*

²*Centre for Astrophysics Research, Department of Physics, Astronomy and Mathematics, University of Hertfordshire, Hatfield, AL10 9AB, UK*

³*European Southern Observatory, Karl-Schwarzschild-Str. 2, 85748 Garching, Germany*

⁴*Max-Planck-Institut für extraterrestrische Physik, Giessenbachstraße, 85748 Garching, Germany*

(Received August 23, 2024; Accepted March 25, 2025)

ABSTRACT

Galaxy chemical enrichment mechanisms have primarily been constrained by $[\alpha/\text{Fe}]$ and $[\text{Fe}/\text{H}]$ measurements of individual stars and integrated light from stellar populations. However such measurements are limited at higher redshifts ($z > 1$). Recently, we proposed an analogous diagram of the oxygen-to-argon abundance ratio, $\log(\text{O}/\text{Ar})$, vs Ar abundance, $12 + \log(\text{Ar}/\text{H})$, as a new diagnostic window for emission nebulae. In this Letter, using line flux measurements including temperature sensitive auroral lines, we present direct determination of O and Ar abundances in nine star-forming galaxies (SFGs) from JWST/NIRSPEC spectra at $z \sim 1.3\text{--}7.7$, and two more with Keck/MOSFIRE spectra at $z \sim 2.2$. Utilising their positions on the $\log(\text{O}/\text{Ar})$ vs $12 + \log(\text{Ar}/\text{H})$ plane, we present the first inference of galaxy chemical enrichment mechanisms from an ensemble of galaxies. Seven SFGs at $z \sim 1.3\text{--}4$ are consistent with the Milky Way solar neighbourhood galactic chemical enrichment models that are driven by core-collapse and Type Ia supernovae in a self-regulated manner. Such enrichment mechanisms thus occur at least out to $z \sim 4$. However, four higher-redshift SFGs ($z \sim 3.6\text{--}7.7$) have lower $\log(\text{O}/\text{Ar})$ values, revealing potentially different enrichment paths becoming important at $z > 3.6$. Such $\log(\text{O}/\text{Ar})$ values may be caused by physical mechanisms such as a rapid but intermittent star-formation and/or additional enrichment sources. This new diagnostic window for SFGs enables us to reveal the unique fingerprints of galaxy chemical enrichment out to cosmic dawn.

Keywords: Chemical abundances (224); Galaxy formation (595); Galaxy chemical evolution (580); James Webb Space Telescope (2291); Supernovae (1668); Milky Way Galaxy (1054)

1. INTRODUCTION

Since the break of cosmic dawn, the interstellar medium (ISM) of galaxies has been continually enriched by the birth and death of stars. The bulk of our understanding of galaxy chemical enrichment (Tinsley 1980; Pagel 1997; Kobayashi et al. 2020a; Matteucci 2021) stems from spectroscopic observations of individual stars in our Milky Way (MW) and studies of nearby galaxies. Deep absorption line spectra of MW stars enabled determination of their $[\text{Fe}/\text{H}]$ and $[\alpha/\text{Fe}]$, revealing the

chemical composition of the ISM at the time of their birth (e.g. Edvardsson et al. 1993; Fuhrmann 1998; Hayden et al. 2015; Imig et al. 2023). The stars showing the highest $[\alpha/\text{Fe}]$ values are thought to have formed at the earliest times from ISM that had only been enriched by core-collapse (CCSNe). Once Type Ia supernovae (SNe Ia) explosions begin, more Fe is released to the ISM than previously, causing a decreasing trend in $[\alpha/\text{Fe}]$ vs $[\text{Fe}/\text{H}]$ for the subsequent generations of stars.

To constrain early chemical enrichment mechanisms, $[\alpha/\text{Fe}]$ and $[\text{Fe}/\text{H}]$ measurements of the oldest generations of stars are required. This is also possible from $[\alpha/\text{Fe}]$ and $[\text{Fe}/\text{H}]$ determined from integrated stellar spectra of early-type galaxies (e.g. Trager et al. 2000;

Thomas et al. 2005; Kuntschner et al. 2010; Greene et al. 2013). At high redshift ($z \sim 2$), only a few quiescent massive galaxies have integrated stellar spectra with sufficiently deep absorption lines to enable determination of $[\alpha/\text{Fe}]$ and $[\text{Fe}/\text{H}]$ (Lonoce et al. 2015; Onodera et al. 2015; Kriek et al. 2016; Beverage et al. 2024a,b). The vast majority of galaxies, however, are star-forming (SFGs) with their fraction increasing with increasing redshift. $[\text{Fe}/\text{H}]$ can also be estimated from rest-frame UV continuum and combined to α abundance from emission lines; $[\alpha/\text{Fe}]$ has been discussed for a few SFGs out to $z \sim 3.4$ (e.g. Steidel et al. 2016; Cullen et al. 2019, 2021; Topping et al. 2020; Stanton et al. 2024).

Recently, the $\log(\text{O}/\text{Ar})$ vs $12 + \log(\text{Ar}/\text{H})$ plane for emission nebulae was found to be analogous to the $[\alpha/\text{Fe}]$ vs $[\text{Fe}/\text{H}]$ plane for stars (Arnaboldi et al. 2022). This was based on the analysis of emission-line spectra of planetary nebulae and HII regions surveyed in the Andromeda galaxy (M 31; Bhattacharya et al. 2019a,b, 2021, 2023) where temperature sensitive auroral lines had been observed (Bhattacharya et al. 2022; Esteban et al. 2020). Like Fe, SNe Ia also preferentially produce more Ar than light α -elements like O, whereas CCSNe produce near-constant $\log(\text{O}/\text{Ar})$, see Kobayashi et al. (2020a). Based on this concept, Arnaboldi et al. (2022) introduced the $\log(\text{O}/\text{Ar})$ vs $12 + \log(\text{Ar}/\text{H})$ plane using planetary nebulae to reveal the chemical enrichment history of M 31 with high star-formation at early times (> 8 Gyr ago) and gas-infall ~ 2 –4 Gyr ago. Kobayashi et al. (2023) then showed that with well-constrained GCE models, the $\log(\text{O}/\text{Ar})$ vs $12 + \log(\text{Ar}/\text{H})$ plane can be connected to the $[\alpha/\text{Fe}]$ - $[\text{Fe}/\text{H}]$ plane.

The spectra of SFGs are dominated by the emission-lines radiated by their constituent HII regions and diffuse ionised gas (Sargent 1970). Using abundance planes derived from their spectra such as $\log(\text{O}/\text{Ar})$ vs $12 + \log(\text{Ar}/\text{H})$ thus opens up the possibility to constrain the chemical enrichment of SFGs.

With the advent of the NIRSPEC multi-slit spectroscopy instrument on board the James Webb Space Telescope (JWST; Jakobsen et al. 2022), direct elemental abundance determination has become possible for a number of SFGs out to $z \sim 8.5$ (e.g. Curti et al. 2023; Nakajima et al. 2023; Sanders et al. 2024) through the detection of the temperature sensitive auroral $[\text{OIII}]\lambda 4363$ Å line. This allows the determination of abundances of a number of elements like O, Ne, S, Ar and N (e.g. Isobe et al. 2023).

These elemental abundances trace the state of the cumulative chemical enrichment of its ISM by previous generations of stars. As we move to higher redshifts, the chemical abundances in galaxies increasingly map

the chemical enrichment from the very early generations of stars. As the relative contribution of CCSNe and SNe Ia varies for the production of distinct elements (see Kobayashi et al. 2020a), we may use the relative abundances of such elements to decipher the state of chemical enrichment of each SFG at their observed redshift.

Rogers et al. (2024) and Welch et al. (2024) determined $\log(\text{O}/\text{Ar})$ values for two SFGs at $z \sim 3$ and $z \sim 1.3$ respectively. Rogers et al. (2024) utilised the aforementioned results (Kobayashi et al. 2020a; Arnaboldi et al. 2022) to interpret the state of chemical enrichment of their individual SFG with a super-solar $\log(\text{O}/\text{Ar})$ value as being primarily enriched by CCSNe. Individual SFGs may occupy different positions in the $\log(\text{O}/\text{Ar})$ vs $12 + \log(\text{Ar}/\text{H})$ plane, and thereby exhibit different states of chemical enrichment. However, by determining the positions of an ensemble of high- z SFGs in this plane, we can constrain the mechanisms that drive early galaxy chemical enrichment.

In this work, we present the state of chemical enrichment in an ensemble of 11 SFGs at $z \sim 1.3$ –7.7 from their O & Ar abundances, providing constraints on the galaxy enrichment mechanisms at these redshifts. The data and determination of O & Ar abundances is presented in Section 2. The positions of these galaxies in the $\log(\text{O}/\text{Ar})$ vs $12 + \log(\text{Ar}/\text{H})$ plane and its implications for early galaxy chemical enrichment is discussed in Section 3. We conclude in Section 4.

2. DATA AND ABUNDANCE DETERMINATION

2.1. Emission-line galaxy sample from MAST

We built a sample of high-redshift ($z > 1$) galaxies with O and Ar abundances determined directly via the detection of temperature sensitive auroral lines. For this purpose, we first identified galaxies that have O abundances published already in the literature from their $[\text{OIII}]\lambda 4363$ Å line detected in JWST/NIRSPEC MOS observations. We then searched for their publicly available¹ 1D JWST/NIRSPEC grating spectra, and verified, via the publicly available automated line fitting algorithm ALFA software (Wesson 2016), whether their $[\text{OIII}]\lambda 4363$ Å line was detected with signal-to-noise $S/N > 3$ in these spectra, using their previously published redshift as an input parameter. We also checked with ALFA whether the ionised Ar lines (either $[\text{ArIII}]\lambda 7136$ Å or $[\text{ArIV}]\lambda\lambda 4711, 4740$ Å) were detected with $S/N > 3$ in these spectra. For the reliability of the flux and wavelength calibration, please see further in Appendix A.

¹ From the Mikulski Archive for Space Telescopes (MAST) at the Space Telescope Science Institute.

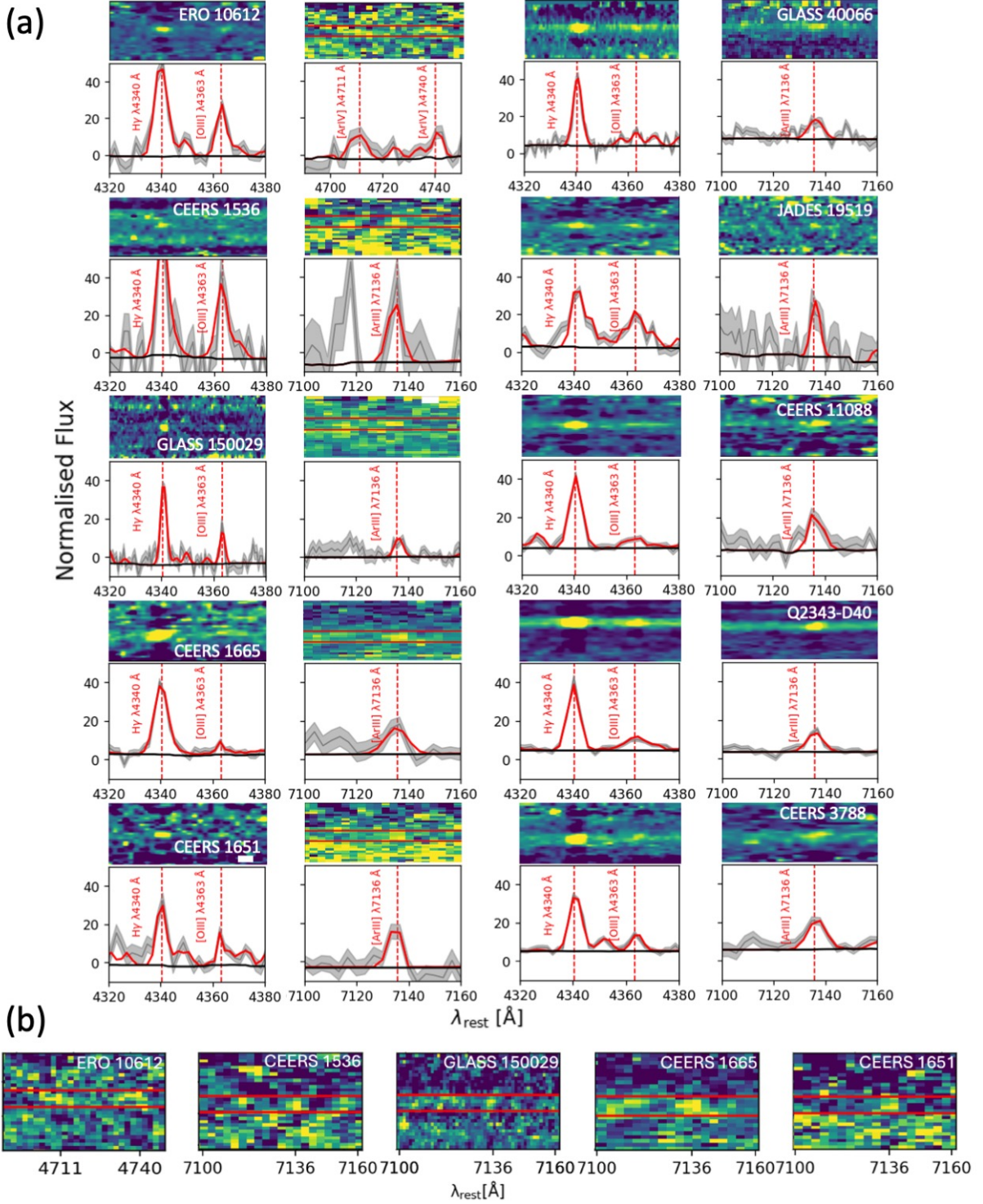


Figure 1. (a) $[\text{OIII}]\lambda 4363 \text{ \AA}$ and ionised Ar lines in flux and wavelength calibrated archival 1D JWST/NIRSPEC spectra and in 2D traces, for the ten galaxies analyzed here. Observed 1D spectra are shown in grey (with shaded 1σ uncertainty), best-fit 1D spectra in red, and fitted continuum in black. For the Argon line regions, the color scale of the 2D traces is adjusted to the line fluxes for the highest redshift (see Table 2) galaxies (left). The horizontal red lines enclose the pixels used by the MAST/JWST pipeline for constructing the 1D spectra. (b) The distribution of line flux to its error ratio ($\text{Flux}/\delta_{\text{Flux}}$) around the detected Ar lines for the same five highest-redshift galaxies; color scale is adapted for each 2D trace. Notice in particular that both $[\text{ArIV}]$ lines are detected for the $z = 7.66$ galaxy ERO 10612 (see also Table 1).

Table 1. Measurements of emission line fluxes (normalised by H β flux of 100) for the 10 galaxies in this work from their archival 1D JWST/NIRSPEC spectra.

Name	[OII] 3726 Å	[OII] 3729 Å	H δ 4102 Å	H γ 4340 Å	[OIII] 4363 Å	[ArIV] 4711 Å	[ArIV] 4740 Å	[OIII] 4959 Å	[OIII] 5007 Å	H α 6563 Å	[SII] 6717 Å	[SII] 6731 Å	[ArIII] 7136 Å
ERO 10612 ^a	14.4 \pm 3.9	—	20.9 \pm 3.6	50.8 \pm 7.4	24.8 \pm 3.7	14.1 \pm 4.1	20.3 \pm 5.1	274.7 \pm 9.3	869.3 \pm 14.9	—	—	—	—
CEERS 1536 ^a	63.8 \pm 12.2	—	—	53.7 \pm 12.1	32.2 \pm 9.1	—	—	252.8 \pm 14.3	795.2 \pm 27.3	628.1 \pm 37.8	—	—	31.4 \pm 9.9
GLASS 150029	17.8 \pm 4.1	20.7 \pm 4.0	25.5 \pm 3.2	39.6 \pm 4.6	18.4 \pm 3.5	—	—	232.8 \pm 9.1	658.8 \pm 15.2	464.3 \pm 11.9	—	—	16.6 \pm 3.2
CEERS 1665	51.2 \pm 2.6	35.2 \pm 2.6	11.8 \pm 1.7	38.3 \pm 3.4	6.7 \pm 2.1	—	—	233.8 \pm 7.9	733.6 \pm 9.3	518.6 \pm 8.9	31.0 \pm 3.1	20.3 \pm 3.9	14.8 \pm 3.9
CEERS 1651 ^b	—	—	—	26.8 \pm 5.9	11.4 \pm 3.6	—	—	217.3 \pm 8.9	636.6 \pm 9.2	—	—	—	28.4 \pm 9.2
GLASS 40066 ^c	—	—	20.1 \pm 1.7	36.8 \pm 2.8	7.8 \pm 1.3	—	—	251.9 \pm 5.5	768.8 \pm 13.4	409.5 \pm 6.2	20.2 \pm 4.2	—	13.3 \pm 2.2
JADES 19519	37.9 \pm 6.1	53.3 \pm 5.9	—	26.2 \pm 4.1	20.1 \pm 4.0	—	—	227.9 \pm 10.5	678.2 \pm 9.2	511.2 \pm 45.1	39.6 \pm 8.3	—	16.7 \pm 3.9
CEERS 11088	52.0 \pm 3.1	47.0 \pm 3.4	14.6 \pm 3.9	38.0 \pm 3.2	8.8 \pm 2.7	—	—	193.6 \pm 3.9	623.3 \pm 7.6	696.6 \pm 22.7	58.3 \pm 7.1	25.7 \pm 7.0	22.9 \pm 5.0
Q2343-D40 ^c	—	—	—	39.7 \pm 2.9	4.0 \pm 1.6	—	—	225.4 \pm 2.3	707.5 \pm 6.9	555.7 \pm 37.8	32.1 \pm 2.9	20.4 \pm 2.9	15.8 \pm 2.1
CEERS 3788	41.7 \pm 1.9	45.9 \pm 1.9	16.0 \pm 2.8	32.2 \pm 2.5	8.8 \pm 1.6	—	—	237.0 \pm 5.4	701.0 \pm 8.2	608.7 \pm 9.5	37.2 \pm 5.6	23.3 \pm 5.8	19.8 \pm 3.5

NOTE—^aFor these galaxies, the [OII] λ 3726, 3729 Å doublet appears blended and its total flux noted in the [OII] λ 3726 Å column.

^bFor this galaxy, the [OII] λ 3726, 3729 Å doublet, H α and [SII] λ 6717, 6731 Å doublet lines are in chip-gaps and are hence unobserved.

^cFor these galaxies, the [OII] λ 3726, 3729 Å doublet lines are in chip-gaps and are hence unobserved.

This procedure resulted in a sample of ten $z > 1$ galaxies for which all the emission lines required for direct abundance determination are present with S/N > 3, see Table 1. The selected spectra cover a wide range of exposure times (0.85 – 29.2 hrs) depending on the parent survey; they are shown in Figure 1a. We note that the spectra of GLASS 150029 and GLASS 40066 have higher spectral resolution than those of the other galaxies, as their observations were carried out with the higher resolution G235H and G395H gratings, while the other galaxies were observed with the medium resolution G235M and G395M gratings. For the galaxy ERO 10612, two sets of observations were available from the MAST archive, acquired at different telescope rotation angles. For our analysis, we used the exposure with strong emission lines in the spectra that have symmetric line profiles while the other one with asymmetric line profiles is not used. All the utilized spectra in this study can be accessed via DOI:10.17909/yj93-nc36 from MAST. Two of these galaxies at $z \sim 4.5$ (GLASS 150029 and CEERS 1665), having relatively broad H α lines, have been reported as candidate AGN hosts² by Harikane et al. (2023) while the other eight are SFGs.

ALFA measures emission line fluxes from galaxy spectra, after subtracting a globally fitted continuum, by optimizing the parameters of Gaussian fits to the line profiles using a genetic algorithm; line-blending are also taken into account (see Appendix B). For faint lines, the wavelength positions and line profile shape, constrained from stronger emission lines, are used as additional discriminants from noise peaks reaching comparable counts/fluxes. As an example, Figure 2a shows the 1D spectrum of CEERS 1651 around its [ArIII] λ 7136 Å line. The ionised Ar line as well as the He I λ 7281 Å line (while not of interest in this work) have gaussian-like profiles and are detected as lines by ALFA. No line is detected at the position of the He I λ 7065 Å line (also not of interest in this work) as the S/N at this position is less than 3. Noise peaks showing non-gaussian line profiles are thus rejected by ALFA, even if the S/N at their positions is greater than 3.

Nevertheless, we will further verify both [OIII] λ 4363 Å and ionised Ar line detections by inspecting their 2D spectra as well as via a stacking analysis for the galaxies with faint [ArIII] λ 7136 Å lines, see Section 2.2.

² As the AGN is unresolved for the two sources, it remains unclear if it is responsible for all their emission-line fluxes. We thus include them in our abundance determination analysis assuming a star-forming ionising source but conservatively they are not considered for the ensuing interpretation.

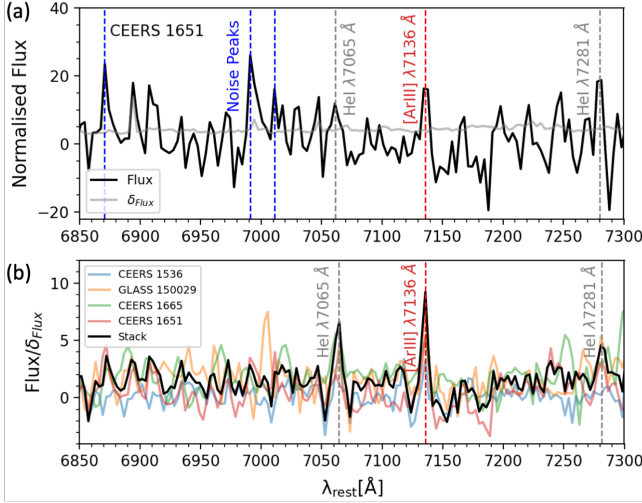


Figure 2. (a) 1D spectrum and flux error for CEERS 1651 as a function of rest-frame wavelength, in a broad wavelength range around the detected [ArIII] λ 7136 Å line. Emission lines with Gaussian like profile such as ionised Ar and He I λ 7281 Å line are identified by ALFA, however the He I λ 7065 Å is too weak to be identified. Noise peaks, given their non-gaussian profiles, are not identified as emission lines. (b) The $\text{Flux}/\delta_{\text{Flux}}$ in the 1D spectra plotted as a function of rest-frame wavelength, in a wavelength range around the detected [ArIII] λ 7136 Å line, for the four highest-redshift galaxies where the line is detected. The $\text{Flux}/\delta_{\text{Flux}}$ for the 1D stacked spectrum for these four galaxies is marked in black.

2.2. Emission line verification

In Figure 1a, we show the 2D traces of the spectra for the 10 galaxies selected from the MAST archive, at the rest wavelength of the [OIII] λ 4363 Å lines and ionised Ar lines. The [OIII] λ 4363 Å lines are clearly visible in the 2D traces with varying intensity for all galaxies, with the faintest emission seen for CEERS 11088.

The ionised Ar lines are also visible in the 2D traces for all galaxies. We note that for ERO 10612, GLASS 150029 and CEERS 1651 there are noise peaks of similar intensity in the 2D traces. Along with CEERS 1536 & CEERS 1665, these constitute the highest redshift ($z > 3.6$) galaxies in our sample (see Table 2). For these five galaxies, we additionally investigate the 2D distribution of their flux to flux error ratio, $\text{Flux}/\delta_{\text{Flux}}$, around the rest-frame wavelengths of their detected ionised Ar lines, see Figure 1b.

For each galaxy, the $\text{Flux}/\delta_{\text{Flux}}$ 2D traces display peaks at the wavelengths of the ionised Ar lines ([ArIV] $\lambda\lambda$ 4711, 4740 Å for ERO 10612 and [ArIII] λ 7136 Å for the others) within the region bracketed by the red lines in Figure 1b, where the 1D spectrum is extracted. Some off-centered peaks are also visible for CEERS 1536 and CEERS 1665 at $\sim 20 - 30$ Å bluer wavelength than the

detected Ar line in Figure 1b. These peaks have sharp profiles which are different from that of the faint line emissions, which are spread on several pixels instead, and better centered within the extraction region.

Finally, to further verify the detection of the [ArIII] λ 7136 Å line fluxes in the publicly available JWST/NIRSPEC spectra for the five highest redshift galaxies in our sample, we computed the stacked 1D spectrum from the individual 1D spectra of CEERS 1536, GLASS 150029, CEERS 1665 and CEERS 1651, adopting the spectral resampling using SpectRes (Carnall 2017) and normalised to their [ArIII] λ 7136 Å line fluxes. In the rest frame 1D stacked spectrum, the S/N of a detected line should show an increase proportional to the square root of the number of stacked spectra in case of Poissonian noise (e.g. Arnaboldi et al. 2002). The $\text{Flux}/\delta_{\text{Flux}}$ in the 1D spectra around the [ArIII] λ 7136 Å lines, for the four galaxies and their 1D spectral stack is shown in Figure 2b. We find that the [ArIII] λ 7136 Å line is detected with S/N of 9.27, showing the expected rough increase in S/N compared to the S/N of the line in individual spectra. In the stacked spectrum the He I λ 7065 Å line is also clearly seen.

Note that for ERO 10612 ($z = 7.66$), the [ArIII] λ 7136 Å line lies beyond the red wavelength limit of NIRSPEC, instead both [ArIV] $\lambda\lambda$ 4711, 4740 Å are independently detected, each with $\text{S/N} \sim 3 - 4$, see Table 1. In the second exposure for ERO 10612 acquired at a different telescope rotator angle, only the [ArIV] λ 4711 Å line is detected with $\text{S/N} \sim 3.75$. The stacked 1D spectra from the two exposures shows that the $\text{Flux}/\delta_{\text{Flux}}$ of the [ArIV] λ 4711 Å line is higher in the stack ($\text{S/N} \sim 4.68$) than in the individual exposures (3.17 and 3.73) by $\approx \sqrt{2}$, supporting a robust detection for this line emission.

2.3. Flux measurements and final sample

For the 10 galaxies above with extracted 1D JWST/NIRSPEC grating spectra, flux measurements of the detected emission-lines are then carried out using ALFA (Wesson 2016). Therefore noise peaks at random wavelengths are never fit, and the wavelengths of all expected fainter lines are known from the bright lines. All lines are fitted to a Gaussian profile iterated during the fit. Since the emission line profile is approximately Gaussian, while the noise peak profile is generally not, even in the unlikely event that a noise peak falls exactly at the wavelength of an expected emission line, a correspondingly large residual will cause a low final S/N, hence a non-detection. The line flux ratios for the emission lines of interest with respect to $\text{H}\beta$ are reported in

Table 2. Physical parameters and abundances of galaxies with $z=1.3\text{--}7.7$ studied in this work.

Name	z	$\log(M_*)$ [M_\odot]	$\log(\text{sSFR})$ [yr^{-1}]	t_{SF} [Myr]	$c(\text{H}\beta)$	T_e [K]	n_e [cm^{-3}]	$12+\log(\text{O}/\text{H})$	$12+\log(\text{Ar}/\text{H})$	$\log(\text{O}/\text{Ar})$
ERO 10612	7.66	7.78 ± 0.29	-6.64 ± 0.29	$4.37^{4.13}_{2.13}$	0.15 ± 0.11	18800 ± 1700	1030 ± 710	7.73 ± 0.08	5.98 ± 0.1	1.75 ± 0.17
CEERS 1536	5.038	8.85 ± 1.09	-7.65 ± 1.11	$44.67^{530.77}_{41.2}$	1.12 ± 0.19	33600 ± 5200	1000^c	7.36 ± 0.04	5.34 ± 0.14	2.02 ± 0.15
GLASS 150029 ^a	4.584	9.12 ± 0.33	-8.08 ± 0.33	$120.23^{136.81}_{63.99}$	0.71 ± 0.11	21100 ± 2600	286 ± 285	7.53 ± 0.08	5.51 ± 0.1	2.02 ± 0.13
CEERS 1665 ^a	4.488	9.79 ± 0.92	-7.37 ± 0.92	$23.44^{171.54}_{20.62}$	1.5 ± 0.28	12900 ± 1700	836 ± 200	8.13 ± 0.1	5.67 ± 0.11	2.46 ± 0.15
CEERS 1651	4.382	8.85 ± 0.89	-7.37 ± 0.9	$23.44^{162.77}_{20.49}$	1.57 ± 0.62	20400 ± 4600	1000^c	7.49 ± 0.16	5.25 ± 0.22	2.23 ± 0.26
GLASS 40066	4.02	9.4 ± 0.31	-7.83 ± 0.31	$67.61^{70.43}_{34.5}$	0.55 ± 0.04	12700 ± 800	1000^c	8.08 ± 0.06	5.65 ± 0.08	2.4 ± 0.11
JADES 19519	3.604	8.64 ± 0.1	-8.04 ± 0.14	$109.65^{41.71}_{30.21}$	0.94 ± 0.16	23700 ± 3400	569 ± 559	7.48 ± 0.08	5.3 ± 0.12	2.18 ± 0.16
CEERS 11088	3.302	9.68	-7.35	22.39	1.37 ± 0.08	15700 ± 2300	606 ± 152	7.87 ± 0.11	5.45 ± 0.11	2.42 ± 0.16
Q2343-D40	2.963	—	—	—	1.03 ± 0.1	13000 ± 1400	68 ± 67	8.01 ± 0.09	5.5 ± 0.09	2.5 ± 0.13
CEERS 3788	2.295	9.45	-8.82	660.69	0.93 ± 0.3	15300 ± 1300	197 ± 53	7.91 ± 0.07	5.56 ± 0.09	2.35 ± 0.11
COSMOS 19985 ^b	2.188	10.12 ± 0.04	-7.8 ± 0.06	$63.1^{9.35}_{8.14}$	0.52 ± 0.09	13640 ± 2900	195 ± 71	7.89 ± 0.2^b	5.33 ± 0.24^b	2.58 ± 0.31^b
COSMOS 20062 ^b	2.185	10.1 ± 0.07	-7.68 ± 0.08	$47.86^{9.68}_{8.05}$	0.68 ± 0.13	8900 ± 2700	231 ± 64	8.24 ± 0.27^b	5.58 ± 0.31^b	2.66 ± 0.41^b
SGAS1723+34 ^b	1.329	8.77 ± 0.15	-7.88 ± 0.16	$75.86^{33.79}_{23.28}$	0.07 ± 0.04	12300 ± 600	130 ± 113	8.13 ± 0.03^b	5.69 ± 0.06^b	2.43 ± 0.08^b

NOTE—Column 1: Name of galaxy; Column 2: galaxy redshift; Column 3–5: Estimated mass, sSFR, and star-formation timescale of galaxies, from their SED fitted to broad-band photometry (see Appendix D); Column 6: Measured Balmer decrement; Column 7: Estimated nebular temperature; Column 8: Estimated electron density; Columns 9–11: Estimated elemental abundances.

^aIdentified from broad $\text{H}\alpha$ lines as AGN host by Harikane et al. (2023).

^bFor these galaxies, the abundances were estimated from line fluxes published in the literature.

^cFor these galaxies, the n_e value has been assumed.

Table 1 for each of the ten galaxies, with 1D spectra of these galaxies shown in Figure 1a.

In addition to these 10 galaxies, we include three high-redshift SFGs in our sample whose relevant line flux measurements, including ionised O and Ar lines, are published in the literature. One SFG at $z \sim 1.3$ had its O and Ar abundances determined directly based on their $[\text{OIII}]\lambda 4363 \text{ \AA}$ line detection in NIRSPEC IFU observations (Welch et al. 2024). For two SFGs at $z \sim 2.2$, their direct determination of O abundances were based on Keck/MOSFIRE spectra but with temperature sensitive $[\text{OII}]\lambda\lambda 7322, 7332 \text{ \AA}$ line detections, where $[\text{ArIII}]\lambda 7136 \text{ \AA}$ line fluxes were also reported (Sanders et al. 2023). We use the published line-flux measurements for these three additional SFGs to determine their O & Ar abundances.

In summary, we thus have a sample of 13 $z > 1$ emission line galaxies, 3 of them with line flux measurements from the literature, while we measure line fluxes for 10 galaxies from their publicly available 1D JWST/NIRSPEC spectra. For all of them, we determine their O & Ar abundances in this work.

2.4. Abundance determination

For each galaxy in our sample, the emission-line fluxes, whether taken from published sources or measured from publicly available spectra, are then passed to NEAT (Nebular Empirical Analysis Tool; Wesson et al. 2012), which applies an empirical scheme to calculate the extinction and elemental abundances. NEAT calculates the intrinsic $c(\text{H}\beta)$ using the flux-weighted ratios of

$\text{H}\alpha/\text{H}\beta$, $\text{H}\gamma/\text{H}\beta$ and $\text{H}\delta/\text{H}\beta$ (whichever pairs are observed) and the extinction law of Cardelli et al. (1989), first assuming a nebular temperature of 10000K and an electron density of 1000 cm^{-3} , and then recalculating $c(\text{H}\beta)$ at the measured temperature and density.

Emission lines fluxes for each galaxy are de-reddened using the calculated $c(\text{H}\beta)$, see Table 2, and their temperatures and densities are calculated using an iterative process from the relevant diagnostic lines using NEAT (see Wesson et al. 2012, section 3.3). For our observations, NEAT utilizes the temperature-sensitive $[\text{OIII}]\lambda 4363 \text{ \AA}$ line, or the $[\text{OII}]\lambda\lambda 7322, 7332 \text{ \AA}$ lines for the two Keck/MOSFIRE observed galaxies, and the density-sensitive $[\text{OII}]\lambda\lambda 3726, 3729 \text{ \AA}$, $[\text{ArIV}]\lambda\lambda 4711, 4740 \text{ \AA}$ and $[\text{SII}]\lambda\lambda 6717, 6731 \text{ \AA}$ doublets to obtain temperature and electron density for each galaxy spectrum. For three galaxies (see Table 2), we do not observe the required doublets to determine electron densities. In these cases, 1000 cm^{-3} is adopted, however the value is expected to have negligible impact on the determined abundances as the emissivities of the auroral line transitions are nearly density independent at the low densities determined for our observed sources (e.g. Ferland et al. 2013). Assuming a lower electron density of 200 cm^{-3} , similar to many galaxies in our sample (see Table 2) leads to consistently lower $\log(\text{O}/\text{Ar})$ values of ~ 0.05 dex and higher $12 + \log(\text{Ar}/\text{H})$ values by ~ 0.03 dex, well within the estimated errors.

O and Ar ionic abundances are measured from the observed fluxes of the O ($[\text{OII}]\lambda\lambda 3726, 3729 \text{ \AA}$, $[\text{OIII}]\lambda\lambda$

4363, 4959, 5007 Å) and Ar ([ArIII] λ 7136 Å and/or [ArIV] $\lambda\lambda$ 4711, 4740 Å) lines respectively. Ionisation correction factor (ICF) for O is negligible when lines pertaining to both O^{2+} (i.e., [OIII] $\lambda\lambda$ 5007, 4959, 4363 Å) and O^+ ([OII] $\lambda\lambda$ 3727, 3729 Å) are observed. Elemental Ar abundances are obtained from the Ar^{2+} ionic abundances utilising the ICF from Amayo et al. (2021) when [ArIII] λ 7136 Å is detected. Only for ERO 10612, the reported Ar abundance is the Ar^{3+} ionic abundance obtained from [ArIV] $\lambda\lambda$ 4711, 4740 Å observations with no ICF correction. The impact of the assumed ICF on the determined Ar abundances and thereby the implications for our results are discussed in Appendix C. Uncertainties are propagated through all steps of the analysis into the final abundance values. Along with the O and Ar abundances in Table 2, we report the galaxy stellar masses, specific-star-formation rates (sSFR) and star-formation timescales (t_{SF}), which are also discussed in Appendix D.

2.5. Comparison with previously published abundance determinations

In Figure 3 we show our determined O abundances against previously published values. Most of our galaxies (Curti et al. 2023: ERO 10612; Sanders et al. 2024: CEERS 1665, Isobe et al. 2023: GLASS 40066; Morishita et al. 2024: JADES 19519; Rogers et al. 2024: Q2343-D40; Sanders et al. 2023: COSMOS 19985, COSMOS 20062; Welch et al. 2024: SGAS1723+34) are consistent within the errors, but some offset is observed for a few others (Nakajima et al. 2023: ERO 10612, CEERS 1536, GLASS 150029; Sanders et al. 2024: CEERS 1651, CEERS 11088, CEERS 3788). Our newly determined $12 + \log(O/H)$ values have a mean offset of 0.09 dex and standard deviation of 0.18 dex compared to the literature values. The small differences are mainly related to differences in flux and wavelength calibration between our utilised archival spectra and those utilised by previous studies. This is illustrated for ERO 10612 where our determined O abundance is consistent with that reported by Curti et al. (2023) but not with that reported by Nakajima et al. (2023), with both these authors using different in-house spectral flux and wavelength calibrations. Indeed, applying our flux measurement and abundance determination procedure to older versions of JWST NIRSPEC spectra for our studied galaxies, as released by previous authors³, we find our determined $12 + \log(O/H)$ values have a lower mean offset of 0.05 dex

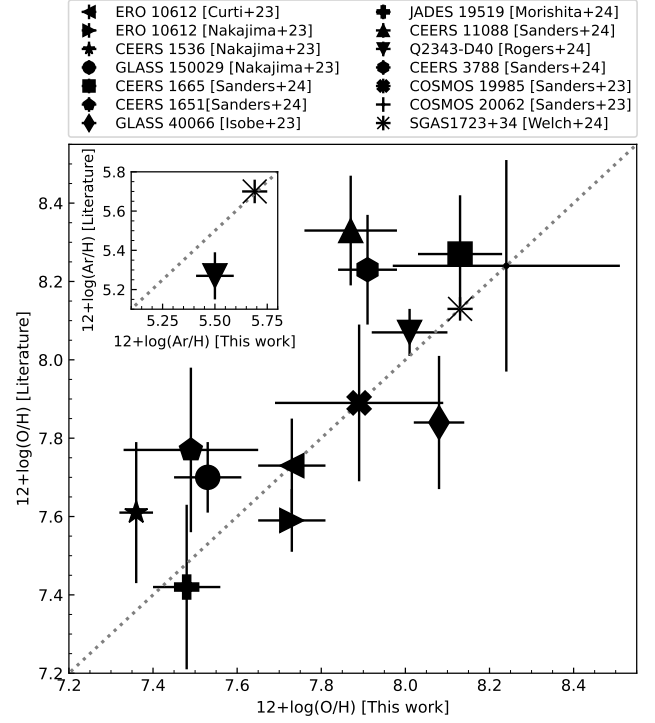


Figure 3. $12 + \log(O/H)$ abundances determined in this work compared to previously published values. The inset shows the same for the two sources with previously published $12 + \log(Ar/H)$ determinations.

and lower standard deviation of 0.06 dex compared to literature works.

We report in this work the first determination of Ar abundances and thereby $\log(O/Ar)$ for all these galaxies except SGAS1723+34 and Q2343-D40. For Q2343-D40, Rogers et al. (2024) reported an Ar abundance slightly lower than our determination, a potential consequence of their choice for a different ICF scheme (Izotov et al. 2006) than that utilised here, or arising from differences in their abundance determination methodology. For SGAS1723+34, Welch et al. (2024) report an Ar abundance nearly identical to our determination (see Figure 3 [inset]).

3. GALAXY CHEMICAL ENRICHMENT AT $Z \sim 1.3-7.7$

Figure 4 [Left] shows the position of the galaxies at $z \sim 1.3-7.7$ in the $\log(O/Ar)$ vs $12 + \log(Ar/H)$ plane, and represents their state of chemical enrichment.

Seven SFGs ($z \sim 1.3-4$; see Figure 4 [Left]) are consistent within error with the Milky Way (MW) solar neighbourhood Galactic Chemical Evolution (GCE) model (Kobayashi et al. 2020a), where CCSNe (including hypernovae) and SNe Ia dominate in a self-regulated scenario with no inflows or outflows. Additionally, their

³ Particularly public versions of the spectra for CEERS DR0.7 and JADES DR3 were analysed.

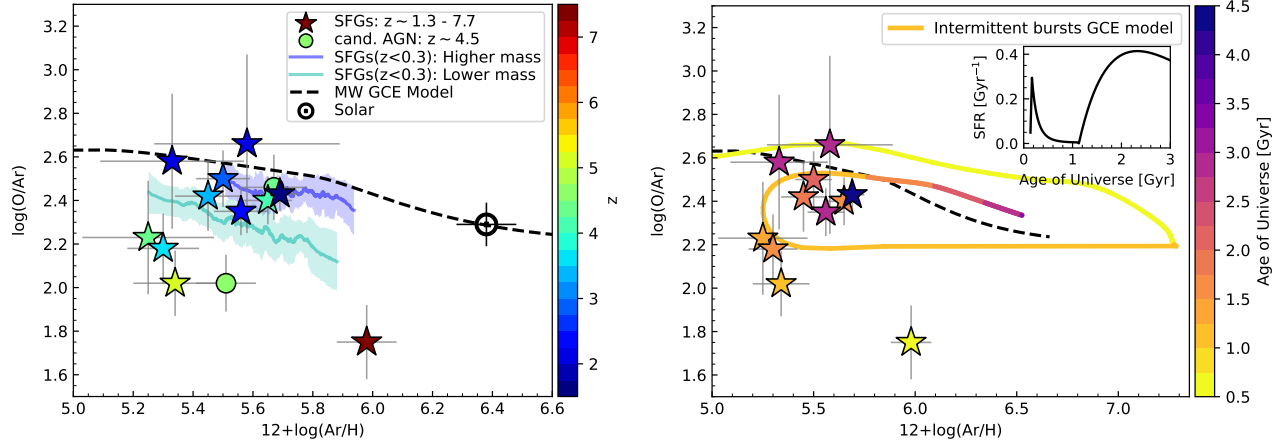


Figure 4. [Left] $\log(\text{O}/\text{Ar})$ vs $12+\log(\text{Ar}/\text{H})$ for the 11 SFGs at $z \sim 1.3-7.7$ and two candidate AGN hosts at $z \sim 4.5$. The galaxies are coloured by their redshift. The green and blue lines respectively show the sequence of mean values of low-redshift ($z < 0.3$) relatively lower mass ($\langle \log(M_*/M_\odot) \rangle = 7.23$) and higher mass ($\langle \log(M_*/M_\odot) \rangle = 9.41$) galaxies from SDSS (Bhattacharya et al. in prep). Their standard deviations are shaded. The MW solar neighbourhood GCE model (Kobayashi et al. 2020a) is shown as black dashed line. [Right] Same as [Left] but now the SFGs are coloured by the age of the universe at their redshift and the AGN candidates are not plotted. Also plotted is a GCE model for an intermittent starburst scenario, that follows the star-formation history shown in the inset, coloured by age of the universe.

position is consistent with the locus traced by the mean $\log(\text{O}/\text{Ar})$ as a function of $12+\log(\text{Ar}/\text{H})$ for the higher mass ($\langle \log(M_*/M_\odot) \rangle = 9.41$) low-redshift ($z < 0.3$) starbursts from SDSS (Brinchmann et al. 2004, Bhattacharya et al. in prep). This remarkably shows that, just like the MW ISM (Matteucci 2021; Kobayashi et al. 2020a) and higher-mass starbursts at $z < 0.3$, the SFGs in our sample out to $z \sim 4$ are consistent with having chemical enrichment being driven mainly by CCSNe and SNe Ia, with the same nucleosynthesis yields and initial mass functions.

We note that O & Ar abundance determination from JWST/NIRSPEC spectra have now been reported independently for an additional 8 galaxies at $z \sim 1.8-5.2$ by Stanton et al. (2024) and 4 more at $z \sim 3.2-4.7$ by Stiavelli et al. (2024). Almost all these galaxies have $\log(\text{O}/\text{Ar})$ and $12+\log(\text{Ar}/\text{H})$ values consistent with the MW GCE model (see also Figure 5 in Stanton et al. 2024).

The only other SFG (KBSS-LM1, $z=2.396$, Steidel et al. 2016) with direct auroral-line measurements and full-spectral UV-fitting⁴ has $[\text{O}/\text{Fe}] \sim 0.6 \pm 0.13$ at $[\text{Fe}/\text{H}] \sim 1.6$. This is coincident with the MW solar neighbourhood GCE model in the $[\text{O}/\text{Fe}]$ vs $[\text{Fe}/\text{H}]$ plane (see Fig 3 in Kobayashi et al. 2020a), and in ex-

tension consistent with the $z \sim 1.3-4$ SFGs presented in this work.

On the other hand, four SFGs ($z \sim 3.5-7.7$) have $\log(\text{O}/\text{Ar})$ values below the MW GCE model considering also their errors and scatter, and even below the sequence traced by lower-mass ($M < 10^8 M_\odot$) $z < 0.3$ starbursts (Figure 4 [Left]). O and Ar have similar dust condensation temperatures (Savage & Sembach 1996), therefore it is unlikely that their $\log(\text{O}/\text{Ar})$ value is underestimated on account of preferential ejection of only condensed O with dust grains.

Therefore in our small sample of galaxies MW-like self-regulated chemical enrichment sequences and their underlying mechanisms hold up to $z \sim 4$. At $z > 3.5$ or so, SFGs appear to be characterised by higher Ar abundance relative to O. In the following subsections, we discuss possible scenarios that may be responsible for the low $\log(\text{O}/\text{Ar})$ values for the higher redshift galaxies in our sample.

3.1. Potential chemical enrichment from intermittent starbursts at high redshift

Keeping the same assumption of the chemical enrichment recipe for the solar neighbourhood (Kobayashi et al. 2020a), we construct an illustrative GCE model considering two bursts of star-formation at very early times (with substantial infall of pristine gas between the bursts), to try and explain the position of the four low $\log(\text{O}/\text{Ar})$ SFGs in this plane (see Figure 4 [Right]). An intermittent star-formation model has previously been invoked to explain measurements of emission line fluxes

⁴ Other SFGs with $[\text{Fe}/\text{H}]$ determined from full-spectral UV-fitting (e.g. Cullen et al. 2019, 2021; Stanton et al. 2024) have $[\text{O}/\text{H}]$ (in lieu of α abundance) determined from strong-line methods from optical emission-lines, which may be over-estimated if not calibrated against direct methods (Maiolino & Mannucci 2019).

in similar high redshift SFGs (Kobayashi & Ferrara 2024). Note that the purpose of constructing this specific model is to investigate whether the low $\log(\text{O}/\text{Ar})$ values of these galaxies may be explained by considering an extreme star-formation history while keeping the MW-like CCSNe and SNe Ia dominated nucleosynthesis.

In Figure 4 [Right] (inset), the star-formation history of the GCE model is plotted. An initial burst of star formation at the break of cosmic dawn is followed by a quiescent phase up to ~ 1.1 Gyr after the birth of the universe, when the ISM is enriched through continued explosions of Type Ia SNe to very high $12 + \log(\text{Ar}/\text{H})$ values and minimum $\log(\text{O}/\text{Ar})$ values. This is followed by an infall of primordial gas that strongly dilutes the ISM, reducing $12 + \log(\text{Ar}/\text{H})$ keeping $\log(\text{O}/\text{Ar})$ constant, and induces another episode of star-formation that starts re-enriching the ISM. Thus a loop in the $\log(\text{O}/\text{Ar})$ vs $12 + \log(\text{Ar}/\text{H})$ plane (Figure 4 [Right]) is formed which is a signature of gas infall (Spitoni et al. 2019; Arnaboldi et al. 2022; Kobayashi et al. 2023). Other models with less extreme star-formation histories (lower star formation rates with continuous or intermittent star-formation with and without gas infall) will occupy the parameter space within the loop spanned by this extreme model in this plane. The model can successfully explain the positions of three of the SFGs at $z \sim 3.5$ –5 that have $\log(\text{O}/\text{Ar}) \sim 2.1$. Note that SFGs are not expected to appear on the constant $\log(\text{O}/\text{Ar}) \sim 2.1$ line, except for at very low $12 + \log(\text{Ar}/\text{H})$ values, for the model (Figure 4 [Right]) as this signifies the rapid dilution of the ISM and star-formation only follows afterwards.

We note however that ERO 10612, which is the highest redshift galaxy in our sample at $z = 7.66$, i.e., just 672 Myr after the birth of the universe⁵, has a $\log(\text{O}/\text{Ar})$ value ~ 1.8 , that is below the $\log(\text{O}/\text{Ar})$ values reached by the intermittent star-formation model (see Figure 4). Additional physical mechanisms, such as outflows, may be at play for this galaxy. A possible scenario may be one where after the first burst of star-formation the CCSNe ejecta with O and Ar are expelled in an outflow while Ar produced over longer timescales is retained, eventually reaching the observed $\log(\text{O}/\text{Ar})$ value ~ 1.8 .

⁵ We assume Planck cosmological parameters (Planck Collaboration et al. 2020): Hubble constant $H_0 = 67.4 \pm 0.5 \text{ km s}^{-1} \text{ Mpc}^{-1}$, matter density parameter $\Omega_m = 0.315 \pm 0.007$. With these assumptions we determine the age of the universe at given redshifts for the galaxies in our sample in Figure 4 [Right]. We assume epoch of first star formation at $z = 25$, within the expected $z = 20$ –30 range (Bromm et al. 2009). This has been applied to the GCE model shown in Figure 4 [Right] (inset).

It remains to be demonstrated whether CCSNe and SNe Ia dominated chemical enrichment models could explain the low- $\log(\text{O}/\text{Ar})$ value for ERO 10612, especially given the short timespan after the birth of the universe within which such abundance values need to be reached. Future GCE simulations for this galaxy exploring different star-formation histories with inflows and outflows may address this property. Additional sources of chemical enrichment described in literature sources may also potentially be at play, as discussed concisely in the following section.

3.2. Additional potential sources of chemical enrichment at high redshift

A potential mechanism for additional Ar production leading to $\log(\text{O}/\text{Ar})$ -poor stellar populations would be to assume a higher SN Ia rate (e.g. with a higher binary fraction) relative to CCSNe for a given stellar population mass in the early universe, than is seen for the MW solar neighbourhood.

Another potential mechanism for Ar enhancement would be the inclusion of sub-Chandrasekhar mass SNe Ia (sub-Ch SNe Ia; see Kobayashi et al. 2020b and references therein) in the GCE models. These sub-Ch SNe Ia have been suggested to be the main enrichment source for observed MW dwarf spheroidal satellite galaxies, which formed their masses at early times and have been quiescent since (Kirby et al. 2019). GCE models including sub-Ch SNe Ia (Kobayashi et al. 2020b) predict very low $\log(\text{O}/\text{Ar})$, as well as low $[\alpha/\text{Fe}]$, because of the higher occurrence of sub-Ch SNe Ia relative to Ch-mass SNe Ia at early times (after ~ 40 Myr).

Another potential rapid metal enrichment source is pair-instability supernovae (PISNe; Heger & Woosley 2002; Nomoto et al. 2013) that have been predicted to evolve from massive ($> 140 M_\odot$) population III stars (first generation metal-free stars formed from pristine gas) having only ~ 2 Myr (Takahashi et al. 2018) lifespans. However, their metal contribution to the ISM is expected to be visible only for a short time after the first generation of stars formed (Hartwig et al. 2018; Vanni et al. 2023), to be washed-out rapidly (Ji et al. 2015) once CCSNe enrichment processes begin after ~ 20 Myr (Kobayashi et al. 2020a). Given the small, albeit uncertain, t_{SF} value of ERO 10612 (see Table 2), PISNe could in principle explain its low $\log(\text{O}/\text{Ar})$ values based on model PISN O and Ar yields (Takahashi et al. 2018), but only if there has been no mixing with any pre-enriched ISM or mass-loss from pre-existing stars. This possibility underlines the interest in further detailed studies of ERO 10612 and other potentially similar systems. However, in GCE models with conventional assump-

tions, the PISN enrichment causes the rapid decrease of $\log(\text{O}/\text{Ar})$ to very low values at much lower metallicities (Kobayashi et al. in prep).

4. SUMMARY AND CONCLUSIONS

We extend the use of the $\log(\text{O}/\text{Ar})$ vs $12 + \log(\text{Ar}/\text{H})$ plane (Arnaboldi et al. 2022; Kobayashi et al. 2023) for inferring the mechanisms that govern galaxy chemical enrichment to SFGs, offering a direct analogy to the $[\alpha/\text{Fe}]$ vs $[\text{Fe}/\text{H}]$ plane for stars. We robustly obtain line-flux measurements for eight SFGs from their flux and wavelength calibrated 1D JWST/NIRSPEC spectra (see Table 1), in addition to three SFGs where such flux measurements were available from their literature sources (see Section 2). We then directly determine O and Ar abundances for these 11 SFGs at $z \sim 1.3\text{--}7.7$ from observations of temperature sensitive auroral lines (Table 2).

We present their positions in the $\log(\text{O}/\text{Ar})$ vs $12 + \log(\text{Ar}/\text{H})$ plane (Figure 4a). Seven SFGs ($z \sim 1.3\text{--}4$) are consistent within error with a MW-like CCSNe and SNe Ia dominated chemical enrichment model (Kobayashi et al. 2020a). Four SFGs ($z \sim 3.5\text{--}7.7$) are found to be $\log(\text{O}/\text{Ar})$ -poor compared to the other seven aforementioned SFGs and the MW GCE model track (Figure 4).

Thus, in the majority of our small sample of galaxies, MW-like self-regulated chemical enrichment sequences and their underlying mechanisms may be in place as early as $z \sim 1.3\text{--}4$. This is corroborated for independent galaxy samples in Stanton et al. (2024) and Stiavelli et al. (2024).

The low $\log(\text{O}/\text{Ar})$ values of three SFGs at higher redshift ($z \sim 3.5\text{--}5$) may be explained through a tailored GCE model with early intermittent star-formation, but keeping the MW-like CCSNe and SNe Ia dominated chemical enrichment (see Section 3.1). For ERO 10612 ($z=7.66$), deeper observations would improve the S/N of the faint $[\text{ArIV}]\lambda 4740 \text{ \AA}$ line. Exploration of different star-formation histories, potentially with more bursts, considering also inflows and outflows that preferentially eject O and/or additional potential sources of Ar enrichment may be required to explain the low $\log(\text{O}/\text{Ar})$ determined for these galaxies. Dedicated GCE models

will be utilized to better understand the rapid Ar enrichment of these SFGs (Kobayashi et al. in prep).

The ever-improving quality of JWST/NIRSPEC data and upcoming large ground-based spectroscopic surveys (e.g. the Prime Focus Spectrograph galaxy evolution survey at Subaru; Greene et al. 2022), implies that it should be possible to build-up a large sample of SFGs with direct determinations of O and Ar abundances from auroral line-flux measurements. In conjunction with tailored GCE models, such a large sample of galaxies with elemental abundance determinations will enable further refinement in the understanding of galaxy chemical enrichment mechanisms presented in this work. There is, thus, now a new window for constraining galaxy chemical enrichment from present day to the early universe.

We thank the anonymous referee for their very useful comments. SB was supported by the INSPIRE Faculty award (DST/INSPIRE/04/2020/002224), Department of Science and Technology (DST), Government of India. SB and MAR acknowledge support to this research from the European Southern Observatory, Garching, through the 2022 SSDF. SB and OG acknowledge support to this research from Excellence Cluster ORIGINS, which is funded by the Deutsche Forschungsgemeinschaft (DFG, German Research Foundation) under Germany's Excellence Strategy - EXC-2094-390783311. MAR and OG thank the Research School of Astronomy and Astrophysics at ANU for support through their Distinguished Visitor Program in 2024. This work was supported by the DAAD under the Australia-Germany joint research programme with funds from the Australian Ministry for Science and Education. CK acknowledges funding from the UK Science and Technology Facility Council through grant ST/Y001443/1.

Facilities: JWST (NIRSPEC), Keck (MOSFIRE), SDSS

Software: AstroPy (Astropy Collaboration et al. 2013, 2018, 2022), SciPy (Virtanen et al. 2020), NumPy (Oliphant 2015), Matplotlib (Hunter 2007), SpectRes (Carnall 2017), NEAT (Wesson et al. 2012) and ALFA (Wesson 2016).

APPENDIX

A. RELIABILITY OF FLUX AND WAVELENGTH CALIBRATIONS FOR JWST/NIRSPEC SPECTRA

The spectra are flux calibrated with an approximately 15% absolute flux accuracy, while field-dependent variations may be as large as 10% as per the latest JWST/NIRSPEC MOS calibration pipeline. Emission line fluxes estimated

from medium resolution grating spectra seem to consistently have $\sim 10\%$ higher flux values compared to PRISM spectra and NIRCAM photometry (Bunker et al. 2023), although line flux ratios (as used here) seem unaffected. As per the same latest calibrations, wavelength calibration is accurate till ~ 15 km/s and ~ 40 km/s for high and medium resolution gratings respectively. Detector artifacts have been more effectively removed by the pipeline for the latest available spectra.

B. IMPACT OF LINE-BLENDING ON ARGON ABUNDANCES

The majority of the O and Ar lines used in this work are not expected to be blended with other lines. Only the [ArIV] λ 4711 Å line, seen only for ERO 10612 in our sample, may occasionally be blended with the HeI λ 4713 Å line. The genetic fitting algorithm of ALFA fits the observed spectra simultaneously to a number of lines, including the [ArIV] λ 4711 Å and HeI λ 4713 Å lines. Given the spectral resolution and the observed flux distribution ~ 4711 Å for ERO 10612, any observed flux was determined by ALFA to be attributed solely to [ArIV] λ 4711 Å, with no contribution from the HeI λ 4713 Å line (if both lines had contributed to the observed flux, then the flux distribution would have been broader). We note that even if these two lines are blended, and the determined Ar abundance of ERO 10612 is overestimated, any potential correction will result in reducing the Ar abundance while increasing its $\log(\text{O}/\text{Ar})$ by the same value, thereby still keeping the same diagonal offset in Figure 4 from the MW-like chemical enrichment sequence in the $\log(\text{O}/\text{Ar})$ vs $12 + \log(\text{Ar}/\text{H})$ plane.

C. IMPACT OF IONISATION CORRECTION FACTORS ON ARGON ABUNDANCES

For Ar, the ionisation states of Ar^{2+} , Ar^{3+} , and in smaller amounts Ar^+ and Ar^{4+} are possible for an SFG. Hence the ICF correction to the observed ionic abundances is relevant for Ar abundance determination. Arellano-Córdova et al. (2024) found that different ICF schemes, including Amayo et al. (2021) used here, have worked equally well for Ar abundance determination. They found that for $z \sim 0.1$ SFGs with $12 + \log(\text{O}/\text{H}) > 8.2$, ICF correction from observing only [ArIII] λ 7136 Å may underestimate the Ar abundance by up to ~ 0.4 dex in their sample, but no such effect is seen when $12 + \log(\text{O}/\text{H}) < 8.2$. This implies that the resulting $\log(\text{O}/\text{Ar})$ values would be higher than their actual intrinsic values. The ICF correction based on the observation of both [ArIII] and [ArIV] lines is more accurate instead at all $12 + \log(\text{O}/\text{H})$ values (see their Figure 3). Only one of our SFGs (COSMOS 20062) has $12 + \log(\text{O}/\text{H}) > 8.2$ with its Ar abundance value determined from the observed Ar^{2+} lines only. Its Ar abundance value may indeed be underestimated but even considering the maximum offset, its $\log(\text{O}/\text{Ar})$ abundance would still be consistent with MW-like chemical enrichment, as it is the galaxy with the highest $\log(\text{O}/\text{Ar})$ in our sample (see Table 2). Other SFGs with [ArIII] λ 7136 Å detection in our sample have $12 + \log(\text{O}/\text{H}) < 8.2$ and thus no ICF correction bias is expected.

For ERO 10612, we have not utilised any ICF correction as no literature ICF scheme directly provides a recipe for Ar abundance determination when only Ar^{3+} ionic abundance is determined. Even if such a scheme were to come to pass, the Ar abundance of ERO 10612 would only increase by a given value, leading to a reduction in $\log(\text{O}/\text{Ar})$ by the same value, thereby still keeping the same diagonal offset in Figure 4 from the MW-like chemical enrichment sequence in the $\log(\text{O}/\text{Ar})$ vs $12 + \log(\text{Ar}/\text{H})$ plane.

D. STELLAR MASS, SPECIFIC-STAR-FORMATION-RATE AND STAR-FORMATION-TIMESCALES OF THE GALAXY SAMPLE

For all the galaxies with $z > 4$, the stellar mass and sSFR (noted in Table 2) were reported by Nakajima et al. (2023), based on their JWST Spectral Energy Distribution (SED) fitting with assumed initial mass function (IMF) from Chabrier (2003). For JADES 19519, the stellar mass and sSFR based on JWST SEDs was reported by Morishita et al. (2024). For CEERS 11088 and 3788, we instead report the Hubble Space Telescope SED-based (Momcheva et al. 2016) estimates of stellar mass and sSFR with the same assumed IMF. The stellar mass and sSFR for COSMOS 19985 and 20062 (Sanders et al. 2023) and SGAS1723+34 (Florian et al. 2021) are also noted in Table 2 but these estimates are not available for Q2343-D40. Star-formation timescale is computed with the simple approximation of $t_{\text{SF}} = 1/\text{sSFR}$. We note that a top-heavy IMF would reduce the stellar masses of the galaxies by ~ 0.5 dex (Harvey et al. 2024).

REFERENCES

- | | |
|--|--|
| Amayo, A., Delgado-Inglada, G., & Stasińska, G. 2021, MNRAS, 505, 2361, doi: 10.1093/mnras/stab1467 | Arellano-Córdova, K. Z., Berg, D. A., Mingozi, M., et al. 2024, ApJ, 968, 98, doi: 10.3847/1538-4357/ad34cf |
|--|--|

- Arnaboldi, M., Aguerri, J. A. L., Napolitano, N. R., et al. 2002, *AJ*, 123, 760, doi: [10.1086/338313](https://doi.org/10.1086/338313)
- Arnaboldi, M., Bhattacharya, S., Gerhard, O., et al. 2022, *A&A*, 666, A109, doi: [10.1051/0004-6361/202244258](https://doi.org/10.1051/0004-6361/202244258)
- Astropy Collaboration, Robitaille, T. P., Tollerud, E. J., et al. 2013, *A&A*, 558, A33, doi: [10.1051/0004-6361/201322068](https://doi.org/10.1051/0004-6361/201322068)
- Astropy Collaboration, Price-Whelan, A. M., Sipőcz, B. M., et al. 2018, *AJ*, 156, 123, doi: [10.3847/1538-3881/aabc4f](https://doi.org/10.3847/1538-3881/aabc4f)
- Astropy Collaboration, Price-Whelan, A. M., Lim, P. L., et al. 2022, *ApJ*, 935, 167, doi: [10.3847/1538-4357/ac7c74](https://doi.org/10.3847/1538-4357/ac7c74)
- Beverage, A. G., Kriek, M., Suess, K. A., et al. 2024a, *ApJ*, 966, 234, doi: [10.3847/1538-4357/ad372d](https://doi.org/10.3847/1538-4357/ad372d)
- Beverage, A. G., Slob, M., Kriek, M., et al. 2024b, *arXiv e-prints*, arXiv:2407.02556, doi: [10.48550/arXiv.2407.02556](https://doi.org/10.48550/arXiv.2407.02556)
- Bhattacharya, S., Arnaboldi, M., Gerhard, O., et al. 2021, *A&A*, 647, A130, doi: [10.1051/0004-6361/202038366](https://doi.org/10.1051/0004-6361/202038366)
- Bhattacharya, S., Arnaboldi, M., Hammer, F., et al. 2023, *MNRAS*, 522, 6010, doi: [10.1093/mnras/stad1378](https://doi.org/10.1093/mnras/stad1378)
- Bhattacharya, S., Arnaboldi, M., Hartke, J., et al. 2019a, *A&A*, 624, A132, doi: [10.1051/0004-6361/201834579](https://doi.org/10.1051/0004-6361/201834579)
- Bhattacharya, S., Arnaboldi, M., Caldwell, N., et al. 2019b, *A&A*, 631, A56, doi: [10.1051/0004-6361/201935898](https://doi.org/10.1051/0004-6361/201935898)
- . 2022, *MNRAS*, 517, 2343, doi: [10.1093/mnras/stac2703](https://doi.org/10.1093/mnras/stac2703)
- Brinchmann, J., Charlot, S., White, S. D. M., et al. 2004, *MNRAS*, 351, 1151, doi: [10.1111/j.1365-2966.2004.07881.x](https://doi.org/10.1111/j.1365-2966.2004.07881.x)
- Bromm, V., Yoshida, N., Hernquist, L., & McKee, C. F. 2009, *Nature*, 459, 49, doi: [10.1038/nature07990](https://doi.org/10.1038/nature07990)
- Bunker, A. J., Cameron, A. J., Curtis-Lake, E., et al. 2023, *arXiv e-prints*, arXiv:2306.02467, doi: [10.48550/arXiv.2306.02467](https://doi.org/10.48550/arXiv.2306.02467)
- Cardelli, J. A., Clayton, G. C., & Mathis, J. S. 1989, *ApJ*, 345, 245, doi: [10.1086/167900](https://doi.org/10.1086/167900)
- Carnall, A. C. 2017, *arXiv e-prints*, arXiv:1705.05165, doi: [10.48550/arXiv.1705.05165](https://doi.org/10.48550/arXiv.1705.05165)
- Chabrier, G. 2003, *PASP*, 115, 763, doi: [10.1086/376392](https://doi.org/10.1086/376392)
- Cullen, F., McLure, R. J., Dunlop, J. S., et al. 2019, *MNRAS*, 487, 2038, doi: [10.1093/mnras/stz1402](https://doi.org/10.1093/mnras/stz1402)
- Cullen, F., Shapley, A. E., McLure, R. J., et al. 2021, *MNRAS*, 505, 903, doi: [10.1093/mnras/stab1340](https://doi.org/10.1093/mnras/stab1340)
- Curti, M., D'Eugenio, F., Carniani, S., et al. 2023, *MNRAS*, 518, 425, doi: [10.1093/mnras/stac2737](https://doi.org/10.1093/mnras/stac2737)
- Edvardsson, B., Andersen, J., Gustafsson, B., et al. 1993, *A&A*, 275, 101
- Esteban, C., Bresolin, F., García-Rojas, J., & Toribio San Cipriano, L. 2020, *MNRAS*, 491, 2137, doi: [10.1093/mnras/stz3134](https://doi.org/10.1093/mnras/stz3134)
- Ferland, G. J., Porter, R. L., van Hoof, P. A. M., et al. 2013, *RMxAA*, 49, 137, doi: [10.48550/arXiv.1302.4485](https://doi.org/10.48550/arXiv.1302.4485)
- Florian, M. K., Rigby, J. R., Acharyya, A., et al. 2021, *ApJ*, 916, 50, doi: [10.3847/1538-4357/ac0257](https://doi.org/10.3847/1538-4357/ac0257)
- Fuhrmann, K. 1998, *A&A*, 338, 161
- Greene, J., Bezanson, R., Ouchi, M., Silverman, J., & the PFS Galaxy Evolution Working Group. 2022, *arXiv e-prints*, arXiv:2206.14908, doi: [10.48550/arXiv.2206.14908](https://doi.org/10.48550/arXiv.2206.14908)
- Greene, J. E., Murphy, J. D., Graves, G. J., et al. 2013, *ApJ*, 776, 64, doi: [10.1088/0004-637X/776/2/64](https://doi.org/10.1088/0004-637X/776/2/64)
- Harikane, Y., Zhang, Y., Nakajima, K., et al. 2023, *ApJ*, 959, 39, doi: [10.3847/1538-4357/ad029e](https://doi.org/10.3847/1538-4357/ad029e)
- Hartwig, T., Yoshida, N., Magg, M., et al. 2018, *MNRAS*, 478, 1795, doi: [10.1093/mnras/sty1176](https://doi.org/10.1093/mnras/sty1176)
- Harvey, T., Conselice, C., Adams, N. J., et al. 2024, *arXiv e-prints*, arXiv:2403.03908, doi: [10.48550/arXiv.2403.03908](https://doi.org/10.48550/arXiv.2403.03908)
- Hayden, M. R., Bovy, J., Holtzman, J. A., et al. 2015, *ApJ*, 808, 132, doi: [10.1088/0004-637X/808/2/132](https://doi.org/10.1088/0004-637X/808/2/132)
- Heger, A., & Woosley, S. E. 2002, *ApJ*, 567, 532, doi: [10.1086/338487](https://doi.org/10.1086/338487)
- Hunter, J. D. 2007, *Computing In Science & Engineering*, 9, 90, doi: [10.1109/MCSE.2007.55](https://doi.org/10.1109/MCSE.2007.55)
- Imig, J., Price, C., Holtzman, J. A., et al. 2023, *ApJ*, 954, 124, doi: [10.3847/1538-4357/ace9b8](https://doi.org/10.3847/1538-4357/ace9b8)
- Isobe, Y., Ouchi, M., Tominaga, N., et al. 2023, *ApJ*, 959, 100, doi: [10.3847/1538-4357/ad09be](https://doi.org/10.3847/1538-4357/ad09be)
- Izotov, Y. I., Stasińska, G., Meynet, G., Guseva, N. G., & Thuan, T. X. 2006, *A&A*, 448, 955, doi: [10.1051/0004-6361:20053763](https://doi.org/10.1051/0004-6361:20053763)
- Jakobsen, P., Ferruit, P., Alves de Oliveira, C., et al. 2022, *A&A*, 661, A80, doi: [10.1051/0004-6361/202142663](https://doi.org/10.1051/0004-6361/202142663)
- Ji, A. P., Frebel, A., & Bromm, V. 2015, *MNRAS*, 454, 659, doi: [10.1093/mnras/stv2052](https://doi.org/10.1093/mnras/stv2052)
- Kirby, E. N., Xie, J. L., Guo, R., et al. 2019, *ApJ*, 881, 45, doi: [10.3847/1538-4357/ab2c02](https://doi.org/10.3847/1538-4357/ab2c02)
- Kobayashi, C., Bhattacharya, S., Arnaboldi, M., & Gerhard, O. 2023, *ApJL*, 956, L14, doi: [10.3847/2041-8213/acf7c7](https://doi.org/10.3847/2041-8213/acf7c7)
- Kobayashi, C., & Ferrara, A. 2024, *ApJL*, 962, L6, doi: [10.3847/2041-8213/ad1de1](https://doi.org/10.3847/2041-8213/ad1de1)
- Kobayashi, C., Karakas, A. I., & Lugaro, M. 2020a, *ApJ*, 900, 179, doi: [10.3847/1538-4357/abae65](https://doi.org/10.3847/1538-4357/abae65)
- Kobayashi, C., Leung, S.-C., & Nomoto, K. 2020b, *ApJ*, 895, 138, doi: [10.3847/1538-4357/ab8e44](https://doi.org/10.3847/1538-4357/ab8e44)
- Kriek, M., Conroy, C., van Dokkum, P. G., et al. 2016, *Nature*, 540, 248, doi: [10.1038/nature20570](https://doi.org/10.1038/nature20570)
- Kuntschner, H., Emsellem, E., Bacon, R., et al. 2010, *MNRAS*, 408, 97, doi: [10.1111/j.1365-2966.2010.17161.x](https://doi.org/10.1111/j.1365-2966.2010.17161.x)

- Lonocce, I., Longhetti, M., Maraston, C., et al. 2015, MNRAS, 454, 3912, doi: [10.1093/mnras/stv2150](https://doi.org/10.1093/mnras/stv2150)
- Maiolino, R., & Mannucci, F. 2019, A&A Rv, 27, 3, doi: [10.1007/s00159-018-0112-2](https://doi.org/10.1007/s00159-018-0112-2)
- Matteucci, F. 2021, A&A Rv, 29, 5, doi: [10.1007/s00159-021-00133-8](https://doi.org/10.1007/s00159-021-00133-8)
- Momcheva, I. G., Brammer, G. B., van Dokkum, P. G., et al. 2016, ApJS, 225, 27, doi: [10.3847/0067-0049/225/2/27](https://doi.org/10.3847/0067-0049/225/2/27)
- Morishita, T., Stiavelli, M., Grillo, C., et al. 2024, arXiv e-prints, arXiv:2402.14084, doi: [10.48550/arXiv.2402.14084](https://doi.org/10.48550/arXiv.2402.14084)
- Nakajima, K., Ouchi, M., Isobe, Y., et al. 2023, ApJS, 269, 33, doi: [10.3847/1538-4365/acd556](https://doi.org/10.3847/1538-4365/acd556)
- Nomoto, K., Kobayashi, C., & Tominaga, N. 2013, ARA&A, 51, 457, doi: [10.1146/annurev-astro-082812-140956](https://doi.org/10.1146/annurev-astro-082812-140956)
- Oliphant, T. E. 2015, Guide to NumPy, 2nd edn. (USA: CreateSpace Independent Publishing Platform)
- Onodera, M., Carollo, C. M., Renzini, A., et al. 2015, ApJ, 808, 161, doi: [10.1088/0004-637X/808/2/161](https://doi.org/10.1088/0004-637X/808/2/161)
- Pagel, B. E. J. 1997, Nucleosynthesis and Chemical Evolution of Galaxies
- Planck Collaboration, Aghanim, N., Akrami, Y., et al. 2020, A&A, 641, A6, doi: [10.1051/0004-6361/201833910](https://doi.org/10.1051/0004-6361/201833910)
- Rogers, N. S. J., Strom, A. L., Rudie, G. C., et al. 2024, ApJL, 964, L12, doi: [10.3847/2041-8213/ad2f37](https://doi.org/10.3847/2041-8213/ad2f37)
- Sanders, R. L., Shapley, A. E., Topping, M. W., Reddy, N. A., & Brammer, G. B. 2024, ApJ, 962, 24, doi: [10.3847/1538-4357/ad15fc](https://doi.org/10.3847/1538-4357/ad15fc)
- Sanders, R. L., Shapley, A. E., Clarke, L., et al. 2023, ApJ, 943, 75, doi: [10.3847/1538-4357/aca9cc](https://doi.org/10.3847/1538-4357/aca9cc)
- Sargent, W. L. W. 1970, ApJ, 160, 405, doi: [10.1086/150443](https://doi.org/10.1086/150443)
- Savage, B. D., & Sembach, K. R. 1996, ARA&A, 34, 279, doi: [10.1146/annurev.astro.34.1.279](https://doi.org/10.1146/annurev.astro.34.1.279)
- Spitoni, E., Silva Aguirre, V., Matteucci, F., Calura, F., & Grisoni, V. 2019, A&A, 623, A60, doi: [10.1051/0004-6361/201834188](https://doi.org/10.1051/0004-6361/201834188)
- Stanton, T. M., Cullen, F., McLure, R. J., et al. 2024, MNRAS, 532, 3102, doi: [10.1093/mnras/stae1705](https://doi.org/10.1093/mnras/stae1705)
- Steidel, C. C., Strom, A. L., Pettini, M., et al. 2016, ApJ, 826, 159, doi: [10.3847/0004-637X/826/2/159](https://doi.org/10.3847/0004-637X/826/2/159)
- Stiavelli, M., Morishita, T., Chiaberge, M., et al. 2024, arXiv e-prints, arXiv:2412.06517, doi: [10.48550/arXiv.2412.06517](https://doi.org/10.48550/arXiv.2412.06517)
- Takahashi, K., Yoshida, T., & Umeda, H. 2018, ApJ, 857, 111, doi: [10.3847/1538-4357/aab95f](https://doi.org/10.3847/1538-4357/aab95f)
- Thomas, D., Maraston, C., Bender, R., & Mendes de Oliveira, C. 2005, ApJ, 621, 673, doi: [10.1086/426932](https://doi.org/10.1086/426932)
- Tinsley, B. M. 1980, FCPh, 5, 287, doi: [10.48550/arXiv.2203.02041](https://doi.org/10.48550/arXiv.2203.02041)
- Topping, M. W., Shapley, A. E., Reddy, N. A., et al. 2020, MNRAS, 495, 4430, doi: [10.1093/mnras/staa1410](https://doi.org/10.1093/mnras/staa1410)
- Trager, S. C., Faber, S. M., Worthey, G., & González, J. J. 2000, AJ, 119, 1645, doi: [10.1086/301299](https://doi.org/10.1086/301299)
- Vanni, I., Salvadori, S., Skúladóttir, Á., Rossi, M., & Koutsouridou, I. 2023, MNRAS, 526, 2620, doi: [10.1093/mnras/stad2910](https://doi.org/10.1093/mnras/stad2910)
- Virtanen, P., Gommers, R., Oliphant, T. E., et al. 2020, Nature Methods, 17, 261, doi: [10.1038/s41592-019-0686-2](https://doi.org/10.1038/s41592-019-0686-2)
- Welch, B., Olivier, G. M., Hutchison, T. A., et al. 2024, arXiv e-prints, arXiv:2401.13046, doi: [10.48550/arXiv.2401.13046](https://doi.org/10.48550/arXiv.2401.13046)
- Wesson, R. 2016, MNRAS, 456, 3774, doi: [10.1093/mnras/stv2946](https://doi.org/10.1093/mnras/stv2946)
- Wesson, R., Stock, D. J., & Scicluna, P. 2012, MNRAS, 422, 3516, doi: [10.1111/j.1365-2966.2012.20863.x](https://doi.org/10.1111/j.1365-2966.2012.20863.x)